



1 **OpenArray v1.0: A Simple Operator Library for the Decoupling of**
2 **Ocean Modelling and Parallel Computing**

3

4 Xiaomeng Huang^{1,2,3}, Xing Huang^{1,3}, Dong Wang^{1,3}, Qi Wu¹, Shixun Zhang³, Yuwen
5 Chen¹, Mingqing Wang^{1,3}, Yi Li³, Yuan Gao¹, Qiang Tang¹, Yue Chen¹, Zheng Fang¹,
6 Zhenya Song^{2,4}, Guangwen Yang^{1,3}

7

8 ¹ Ministry of Education Key Laboratory for Earth System Modeling, Department of
9 Earth System Science, Tsinghua University, Beijing 100084, China

10 ² Laboratory for Regional Oceanography and Numerical Modeling, Qingdao National
11 Laboratory for Marine Science and Technology, Qingdao, 266237, China

12 ³ National Supercomputing Center in Wuxi, Wuxi, 214011, China

13 ⁴ First Institute of Oceanography, Ministry of Natural Resources, Qingdao, 266061,
14 China

15

16 Corresponding author: hxm@tsinghua.edu.cn

17 **Abstract**

18 The increasing complexity of climate models combined with rapidly evolving
19 computational techniques introduces a large gap in climate modelling. In this work, we
20 design a simple computing library to decouple the work of ocean modelling from the
21 work of parallel computing. The library provides twelve basic operators that feature
22 user-friendly interfaces, effective programming and automatic parallelization. We
23 further implement a highly readable and efficient ocean model that contains only 1860
24 lines of code but achieves a 91% parallel efficiency in strong scaling and 99% parallel
25 efficiency in weak scaling with 4096 Intel CPU cores. This ocean model also exhibits
26 excellent scalability on the Sunway TaihuLight supercomputer. This work presents a
27 valuable example for the development of the next generation of ocean models.

28

29 **Keywords:** automatic parallelization, operator, ocean modelling, parallel computing



30 **1. Introduction**

31 Numerous climate models have been developed in the past several decades to improve
32 the predictive understanding of the climate system (Bonan and Doney, 2018; Collins et
33 al., 2018; Taylor et al., 2012). These models are becoming increasingly complicated,
34 and the amount of code has expanded from a few thousand lines to tens of thousands
35 of lines, or even millions of lines. In terms of software engineering, an increase in code
36 causes the models to be more difficult to develop and maintain.

37

38 The complexity of these models mainly originates from three aspects. First, more model
39 components and physical processes have been embedded into the climate model,
40 leading to a tenfold increase in the amount of code (Alexander and Easterbrook, 2015).
41 Second, some heterogeneous and advanced computing platforms (Lawrence et al., 2018)
42 have been widely applied by the climate community, resulting in a fivefold increase in
43 the amount of code (Xu et al., 2015). Last, most of the model program needs to be
44 rewritten due to the continual development of novel numerical methods and meshes.
45 The promotion of novel numerical methods and technologies produced in the fields of
46 computational mathematics and computer science have been limited in climate science
47 because of the extremely heavy burden caused by program rewriting and migration.

48

49 Over the next few decades, tremendous computing capacities will be accompanied by
50 more heterogeneous architectures, thus making for a much more sophisticated
51 computing environment for climate modellers than ever before (Bretherton et al., 2012).
52 Clearly, transiting the current climate models to the next generation of computing
53 environments will be highly challenging and disruptive. Overall, complex climate
54 model codes combined with rapidly evolving computational techniques create a very
55 large gap in climate science.

56

57 To reduce the complexity of climate models and bridge this gap, we believe that a
58 universal and productive computing library is probably the solution. Through



59 establishing an implicit parallel and platform-independent computing library, the
60 complex models can be simplified and will no longer need explicit parallelization and
61 transiting, thus effectively decoupling the development of ocean models from
62 complicated parallel computing techniques and diverse heterogeneous computing
63 platforms.

64

65 Many studies have addressed the complexity of parallel programming for numerical
66 simulations. Operator overloading is one of the mainstream implementations and is
67 fairly straightforward (Corliss and Griewank, 1994; Walther et al., 2003). However, this
68 method is prone to work inefficiency because overloading execution induces numerous
69 unnecessary intermediate variables, consuming valuable memory bandwidth resources.
70 Using a source-to-source translator offers another solution. The important design
71 philosophy of this method is dependent on the simple self-defined rules in the former
72 language to automatically generate code conforming to the latter language (Bae et al.,
73 2013; Lidman et al., 2012). In the MIT General Circulation Model (MITgcm), the
74 modellers use OpenAD (Naumann et al., 2006; Utke et al., 2008), which is an automatic
75 algorithmic differentiation tool with a set of mathematical and linguistic rules, to
76 generate fairly efficient tangent linear and adjoint code (Adcroft et al., 2017). Moreover,
77 some outstanding domain specific languages (DSL), such as ATMOL (van Engelen,
78 2001), ICON DSL (Torres et al., 2013) and STELLA (Gysi et al., 2015), provide high-
79 level abstraction interfaces that use mathematical notations similar to those used by
80 domain scientists so that they can write much more concise and simpler code.

81

82 In fact, when using source-to-source translator and DSL methods to develop practical
83 climate models, one major difficulty is the requirement of a stable and robust compiler,
84 rather than an experimental compiler, at the product level. Another difficulty is that the
85 climate modellers have to change their programming habits and master a new
86 programming method through novel rules or DSLs instead of using Fortran, which they
87 are most familiar with. The last difficulty is that although a small part of the existing



88 source-to-source translators and DSLs currently support graphics processing units
89 (GPUs), most of the source-to-source translators and DSLs still do not support the
90 rapidly evolving heterogeneous computing platforms, especially the Chinese Sunway
91 TaihuLight supercomputer located at the National Supercomputing Center in Wuxi.

92

93 Inspired by the philosophy of operator overloading, source-to-source translating and
94 DSLs, we integrated the advantages of these three methods into a simple computing
95 library which is called OpenArray. The main contributions of OpenArray are as follows:

- 96 • Easy-to-use. The modellers can write simple operator expressions in Fortran to
97 solve partial differential equations (PDEs). The entire program appears to be
98 serial and the modellers do not need to know any parallel computing techniques.
99 We summarized twelve basic generalized operators to support whole model
100 calculations in ocean models using the finite difference method and staggered
101 grid in OpenArray.
- 102 • High efficiency. We adopt some advanced methods, including intermediate
103 computation graphing, asynchronous communication, kernel fusion, loop
104 optimization, and vectorization, to decrease the consumption of memory
105 bandwidth and improve efficiency. Performance of the programs implemented
106 by OpenArray is similar to that of original parallel program manually optimized
107 by experienced programmers.
- 108 • Portability. The current OpenArray version support both CPU and Sunway
109 platforms. The input of OpenArray is a Fortran source file including the operator
110 expression form; then, the intermediate C++ code is automatically generated by
111 OpenArray. The final output is a program that is executable on different
112 computing platforms.

113

114 Furthermore, we developed a practical ocean model based on the Princeton Ocean
115 Model (POM, Blumberg and Mellor, 1987) to test the capability and efficiency of
116 OpenArray. The new model is called the Generalized Operator Model of the Ocean



117 (GOMO). Because the parallel computing details are completely hidden, GOMO
118 consists of only 1860 lines of Fortran code and is more easily understood and
119 maintained than the original POM. Moreover, GOMO exhibits excellent scalability and
120 portability to central processing unit (CPU) and Sunway platforms.

121

122 The remainder of this paper is organized as follows. Section 2 introduces some concepts
123 and presents the detailed mathematical descriptions of formulating the PDEs into
124 operator expressions. Section 3 describes the detailed design and optimization
125 techniques of OpenArray. Implementation of GOMO is described in section 4. Section
126 5 evaluates the performance of OpenArray and GOMO. Finally, conclusions are given
127 in section 6.

128

129 **2. Concepts of the Array, Operator, and Abstract Staggered Grid**

130 In this section, we introduce three important concepts in OpenArray: Array, Operator
131 and Abstract Staggered Grid to illustrate the design of OpenArray.

132

133 **2.1 Array**

134 To achieve this simplicity, we designed a derived data type, *Array*, which inspired our
135 project name, OpenArray. The new *Array* data type comprises a series of information,
136 including a 3-dimensional array to store data, a pointer to the computational grid, a
137 Message Passing Interface (MPI) communicator, the size of the halo region and other
138 information about the data distribution. All the information is used to manipulate the 3-
139 dimensional array as a complete object to simplify the parallel computing. In the
140 traditional ocean models, calculations for each grid point and the i , j , and k loops in the
141 horizontal and vertical directions are unavoidable. The advantage of taking the arrays
142 as a complete object is the significant reduction in the number of loop operations in the
143 models, making the code more intuitive and readable. When using OpenArray library
144 in a program, one can use `type(Array)` to declare new variables.



145 2.2 Operator

146 To illustrate the concept of an operator, we first take a 2-dimensional (2D) continuous
 147 equation solving sea surface elevation as an example:

$$148 \quad \frac{\partial \eta}{\partial t} + \frac{\partial DU}{\partial x} + \frac{\partial DV}{\partial y} = 0 \quad (1)$$

149 where η is the surface elevation, U and V are the zonal and meridional velocities, and
 150 D is the depth of the fluid column. We choose the finite difference method and staggered
 151 Arakawa C grid scheme, which are adopted by most regional ocean models. Then, the
 152 above continuous equation can be discretized into the following form.

$$153 \quad \frac{\eta_{t+1}(i,j) - \eta_{t-1}(i,j)}{2*dt} + \frac{(D(i+1,j)+D(i,j))*U(i+1,j) - (D(i,j)+D(i-1,j))*U(i,j)}{dx(i,j)} +$$

$$154 \quad \frac{(D(i,j+1)+D(i,j))*V(i,j+1) - (D(i,j)+D(i,j-1))*V(i,j)}{dy(i,j)} = 0 \quad (2)$$

155 where subscripts η_{t+1} and η_{t-1} denote the surface elevations at the $(t+1)$ time step and $(t-$
 156 $1)$ time step. To simplify the discrete form, we introduce some notation for the
 157 differentiation (δ_f^x, δ_b^y) and interpolation ($\overline{(\)}_f^x, \overline{(\)}_b^y$). The δ and overbar symbols define
 158 the differential operator and average operator. The subscript x or y denotes that the
 159 operation acts in the x or y direction, and the superscript f or b denotes that the
 160 approximation operation is forward or backward.

161

162 Table 1 lists the detailed definitions of twelve basic operators. The term *var* denotes a
 163 3-dimensional model variable. All twelve operators for the finite difference calculations
 164 are named using three letters in the form [A|D][X|Y|Z][F|B]. The first letter contains
 165 two options, A or D, indicating an average or a differential operator. The second letter
 166 contains three options, X, Y or Z, representing the direction of operation. The last letter
 167 contains two options, F or B, representing forward or backward operation. The dx , dy
 168 and dz are the distances between two adjacent grid points along the x , y and z directions.
 169 Using the basic operators, Eq. (2) is expressed as:

$$170 \quad \frac{\eta_{t+1} - \eta_{t-1}}{2*dt} + \delta_f^x(\overline{D}_b^x * U) + \delta_f^y(\overline{D}_b^y * V) = 0 \quad (3)$$

171 Thus,

$$172 \quad \eta_{t+1} = \eta_{t-1} - 2 * dt * \left(\delta_f^x(\overline{D}_b^x * U) + \delta_f^y(\overline{D}_b^y * V) \right) \quad (4)$$

173 Then, Eq. (4) can be easily translated into a line of code using operators (the bottom



174 left panel in Fig. 1). Compared with the pseudo-codes (the right panel), the
 175 corresponding implementation by operators is simpler and more consistent with the
 176 equations.

177

178 Next, we will use the operators in shallow water equations, which are more complicated
 179 than those in the previous case. Assuming that the flow is in hydrostatic balance and
 180 that the density and viscosity coefficient are constant, and neglecting the molecular
 181 friction, the shallow water equations are:

$$182 \quad \frac{\partial \eta}{\partial t} + \frac{\partial DU}{\partial x} + \frac{\partial DV}{\partial y} = 0 \quad (5)$$

$$183 \quad \frac{\partial DU}{\partial t} + \frac{\partial DUU}{\partial x} + \frac{\partial DVU}{\partial y} - fVD = -gD \frac{\partial \eta}{\partial x} + \mu D \left(\frac{\partial^2 U}{\partial x^2} + \frac{\partial^2 U}{\partial y^2} \right) \quad (6)$$

$$184 \quad \frac{\partial DV}{\partial t} + \frac{\partial DUV}{\partial x} + \frac{\partial DVV}{\partial y} + fUD = -gD \frac{\partial \eta}{\partial y} + \mu D \left(\frac{\partial^2 V}{\partial x^2} + \frac{\partial^2 V}{\partial y^2} \right) \quad (7)$$

185 where f is the Coriolis parameter, g is the gravitational acceleration, and μ is the
 186 coefficient of kinematic viscosity. Using the Arakawa C grid and leapfrog time
 187 difference scheme, the discrete forms represented by operators are shown in Eq. (8) ~
 188 Eq. (10).

$$189 \quad \frac{\eta_{t+1} - \eta_{t-1}}{2 \cdot dt} + \delta_f^x (\bar{D}_b^x * U) + \delta_f^y (\bar{D}_b^y * V) = 0 \quad (8)$$

$$190 \quad \frac{D_{t+1}U_{t+1} - D_{t-1}U_{t-1}}{2 \cdot dt} + \delta_b^x (\bar{D}_b^x * U_f^x * \bar{U}_f^x) + \delta_f^y (\bar{D}_b^y * V_b^x * \bar{U}_b^y) - f \bar{V}_f^y * D_b^x = -g *$$

$$191 \quad \bar{D}_b^x * \delta_b^x(\eta) + \mu * \bar{D}_b^x * \left(\delta_f^x (\delta_b^x(U_{t-1})) + \delta_f^y (\delta_b^y(U_{t-1})) \right) \quad (9)$$

$$192 \quad \frac{D_{t+1}V_{t+1} - D_{t-1}V_{t-1}}{2 \cdot dt} + \delta_f^x (\bar{D}_b^x * U_b^y * \bar{V}_b^x) + \delta_b^y (\bar{D}_b^y * V_f^y * \bar{V}_f^y) + f \bar{U}_f^x * D_b^y = -g *$$

$$193 \quad \bar{D}_b^y * \delta_b^y(\eta) + \mu * \bar{D}_b^y * \left(\delta_f^x (\delta_b^x(V_{t-1})) + \delta_b^y (\delta_f^y(V_{t-1})) \right) \quad (10)$$

194 As the shallow water equations are solved, spatial average and difference operations
 195 are called repeatedly. Such operations consume the vast majority of the computing
 196 resources when solving the shallow water equations. Therefore, it is necessary to
 197 abstract these common operations from PDEs and encapsulate them into user-friendly,
 198 platform-independent implicit parallel operators. As shown in Fig. 2, we require only 3
 199 lines of code to solve the shallow water equations. This more realistic case suggests



200 that even more complex PDEs can be constructed and solved by following this elegant
201 approach.

202

203 **2.3 Abstract staggered grid**

204 Most ocean models are implemented on the basis of the staggered Arakawa grids
205 (Arakawa and Lamb, 1981; Griffies et al., 2000). The variables in ocean models are
206 allocated at different grid points. The calculations that use these variables are performed
207 after several reasonable interpolations or differences. When we call the differential
208 operations on a staggered grid, the difference value between adjacent points should be
209 divided by the grid increment to obtain the final result. Setting the correct grid
210 increment for modellers is troublesome work that is extremely prone to error, especially
211 when the grid is nonuniform. Therefore, we proposed an abstract staggered grid to
212 support flexible switching of operator calculations among different staggered grids.
213 When the grid information is provided at the initialization phase of OpenArray, the
214 operators can automatically set the correct grid increments for different *Array* variables.
215

216 As shown in Fig. 3, the cubes in the (a), (b), (c), and (d) panels are the minimum abstract
217 grid accounting for 1/8 of the volume of cube in the (e) panel. The eight points of each
218 cube are numbered sequentially from 0 to 7, and each point has a set of grid increments,
219 i.e., dx , dy and dz . For example, all the variables of an abstract Arakawa A grid are
220 located at Point 3. For the Arakawa B grid, the horizontal velocity *Array* (U , V) are
221 located at Point 0, the temperature (T), the salinity (S), and the depth (D) are located at
222 Point 3, and the vertical velocity *Array* (W) is located at Point 7. For the Arakawa C
223 grid, *Array* U is located at Point 2 and *Array* V is located at Point 1. In contrast, for the
224 Arakawa D grid, *Array* U is located at Point 1 and *Array* V is located at Point 2.

225

226 When we call the average and differential operators mentioned in Table 1, for example,
227 on the abstract Arakawa C grid, the position of *Array* D is Point 3, and the average AXB
228 operator acting on *Array* D will change the position from Point 3 to Point 1. Since *Array*



229 U is also allocated at Point 1, the operation $AXB(D)*U$ is allowed. In addition, the
230 subsequent differential operator on *Array* $AXB(D)*U$ will change the position of *Array*
231 $DXF(AXB(D)*U)$ from Point 1 to Point 3.

232

233 The jumping rules of different operators are given in Table 2. Due to the design of the
234 abstract staggered grids, the jumping rules for the Arakawa A, B, C, and D grids are
235 fixed. A change in the position of an array is determined only by the direction of a
236 certain operator acting on that array.

237

238 The position information and jumping rules can be used to automatically check whether
239 the discrete form of an equation is correct. The grid increments are hidden by all the
240 differential operators, making the code simple and clean. In addition, since the rules are
241 suitable for multiple staggered Arakawa grids, the modellers can flexibly switch the
242 ocean model between different Arakawa grids. Notably, the users of OpenArray should
243 input the correct positions of each array in the initialization phase. The value of the
244 position is an input parameter when declaring an *Array*. An error will be reported if an
245 operation is performed between misplaced points.

246

247 Although most of the existing ocean models use finite difference or finite volume
248 methods on structured or semi-structured meshes, such as POM, the Modular Ocean
249 Model (MOM) (Griffies, 2012), the Parallel Ocean Program (POP) (Smith et al., 2010),
250 MITgcm (Adcroft et al., 2017), and the Regional Ocean Modeling System (ROMS)
251 (Shchepetkin and McWilliams, 2005), there are still some ocean models using
252 unstructured meshes, including Advanced Circulation model (ADCIRC) (Luettich et
253 al., 1992), Finite-Volume Coastal Ocean Model (FVCOM) (Chen et al., 2003), and
254 Stanford Unstructured Nonhydrostatic Terrain-following Adaptive Navier-Stokes
255 Simulator (SUNTANS) (Fringer et al., 2006), and even the spectral element method
256 (e.g. Levin et al., 2000). In our current work, we design the basic operator only for finite
257 different and finite volume methods with structured grids. More customized operator



258 for the other numerical methods and meshes will be implemented in our future work.

259

260 **3. Design of OpenArray**

261 Through the above operator notations in Table 1, ocean modellers can quickly convert
262 the discrete PDE equations into the corresponding operator expression forms. The main
263 purpose of OpenArray is to make complex parallel programming transparent to the
264 modellers. As illustrated in Fig. 4, we use a computation graph as an intermediate
265 representation, meaning that the operator expression forms written in Fortran will be
266 translated into a computation graph with a particular data structure. In addition,
267 OpenArray will use the intermediate computation graph to analyse the dependency of
268 the distributed data and automatically produce the underlying parallel code. Finally, we
269 use stable and mature compilers, such as the GNU Compiler Collection (GCC), Intel
270 compiler (ICC), and Sunway compiler (SWACC), to generate the executable program
271 according to different backend platforms. These four steps and some related techniques
272 are described in detail in this section.

273

274 **3.1 Operator expression**

275 Although the basic generalized operators listed in Table 1 are only suitable to execute
276 first-order difference, other high-order difference or even more complicated operations
277 can be combined by these basic operators. For example, a second-order difference
278 operation can be expressed as $\delta_f^x(\delta_b^x(var))$. Supposing the grid distance is uniform,
279 the corresponding discrete form is $[var(i+1,j,k)+var(i-1,j,k) - 2* var(i,j,k)] / dx^2$. In
280 addition, the central difference operation can be expressed as $(\delta_f^x(var) + \delta_b^x(var))/2$
281 since the corresponding discrete form is $[var(i+1,j,k)-var(i-1,j,k)] / 2dx$.

282

283 Using these operators to express the discrete PDE equation, the code and formula are
284 very similar. We call this effect “the self-documenting code is the formula”. Fig. 5
285 shows the one-to-one correspondence of each item in the code and the items in the sea
286 surface elevation equation. The code is very easy to program and understand. Clearly,



287 the basic operators and the combined operators greatly simplify the development and
288 maintenance of ocean models. The complicated parallel and optimization techniques
289 will be concealed by these operators. Modellers no longer need to care about details
290 and escape from the “parallelism swamp”, thus they can concentrate on the scientific
291 issues.

292

293 **3.2 Intermediate computation graph**

294 Considering the example mentioned in Fig. 5, if one needs to compute the term
295 $DXF(AXB(D)*u)$ with the traditional operator overloading method, one first computes
296 $AXB(D)$ and stores the result into a temporary array (named $tmp1$), and then executes
297 $(tmp1*u)$ and stores the result into a new array, $tmp2$. The last step is to compute
298 $DXF(tmp2)$ and store the result in a new array, $tmp3$. Numerous temporary arrays
299 consume a considerable amount of memory, making the efficiency of operator
300 overloading is poor.

301

302 To solve this problem, we convert an operator expression form into a directed and
303 acyclic graph, which consists of basic data and function nodes, to implement a lazy
304 expression evaluation (Bloss et al., 1988; Reynolds, 1999). Unlike the traditional
305 operator overloading method, we overload all arithmetic functions to generate an
306 intermediate computation graph rather than to obtain the result of each function. This
307 method is widely used in deep learning frameworks, e.g., TensorFlow (Abadi et al.,
308 2016) and Theano (Bastien et al., 2012), to improve computing efficiency. Figure 6
309 shows the procedure of parsing the operator expression form of the sea level elevation
310 equation into a computation graph. The input variables in the square boxes include the
311 sea surface elevation (elb), the zonal velocity (u), the meridional velocity (v) and the
312 depth (D). $dt2$ is a constant equal to $2*dt$. The final output is the sea surface elevation
313 at the next time step (elf). The operators in the round boxes have been overloaded in
314 OpenArray. In summary, all the operators provided by OpenArray are functions for the
315 Array calculation, in which the “=” notation is the assignment function, the “-” notation
316 is the subtraction function, the “*” notation is the multiplication function, the “+”



317 notation is the addition function, DXF and DYF are the differential functions, and AXF
318 and AYF are the interpolated functions.

319

320 **3.3 Automatic code generation**

321 Given a computation graph, we design a lightweight engine to automatically generate
322 the corresponding source code automatically (Fig. 7). Each operator node in the
323 computation graph is called a kernel. The sequence of all kernels in a graph is usually
324 fused into a large kernel function. Therefore, the underlying engine schedules and
325 executes the fused kernel once and obtains the final result directly without any auxiliary
326 or temporary variables. Simultaneously, the scheduling overhead of the computation
327 graph and the startup overhead of the basic kernels can be reduced.

328

329 Most of the scientific computational applications are limited by the memory bandwidth
330 and cannot fully exploit the computing power of a processor. Fortunately, kernel fusion
331 is an effective optimization method to improve memory locality. When two kernels
332 need to process some data, their fusion holds shared data in the memory. Prior to the
333 kernel fusion, the computation graph is automatically analysed to find the operator
334 nodes that can be fused, and the analysis results are stored in several subgraphs. After
335 being given a series of subgraphs, the underlying engine dynamically generates the
336 corresponding kernel function in C++ using just-in-time (JIT) compilation techniques
337 (Suganuma and Yasue, 2005). Notably, the time to compile a single kernel function is
338 short, but practical applications usually need to be run for thousands of time steps, and
339 the overhead of generating and compiling the kernel functions for the computation
340 graph is extremely high. Therefore, we generate a fusion kernel function only once for
341 each subgraph, and put it into a function pool. Later, when facing the same computation
342 subgraph, we fetch the corresponding fusion kernel function directly from the pool.

343

344 Since the arrays in OpenArray are distributed among different processing units, and the
345 operator needs to use the data in the neighbouring points, in order to ensure the



346 correctness, it is necessary to check the data consistency before fusion. The use of
347 different data splitting methods for distributed arrays can greatly affect computing
348 performance. The current data splitting method in OpenArray is the widely used block-
349 based strategy. Solving PDEs on structured grids often divides the simulated domain
350 into blocks that are distributed to different processing units. However, the difference
351 and average operators always require their neighbouring points to perform array
352 computations. Clearly, controlling the communication of the boundary region is tedious
353 work for ocean modellers.

354

355 Therefore, we implemented a general boundary management module to automatically
356 maintain and update the boundary information so that the modellers no longer need to
357 address the message communication. The boundary management module uses
358 asynchronous communication to update and maintain the data of the boundary region,
359 which is useful for simultaneous computing and communication. These procedures of
360 asynchronous communication are implicitly invoked when calling the basic kernel or
361 the fused kernel to ensure that the parallel details are completely transparent to the
362 modellers.

363

364 **3.4 Portable program for different backend platforms**

365 With dynamic code generation and JIT compilation technology, OpenArray can be
366 easily migrated to different backend platforms. Currently, we have designed the
367 corresponding source code generation module for Intel CPU and Sunway processors in
368 OpenArray.

369

370 The Sunway TaihuLight is the third fastest supercomputer in the world, with a
371 LINPACK benchmark rating of 93 Petaflops provided by a multi-core Sunway
372 processor that includes 4 core-groups, each of which consists of 64 computing
373 processing elements (CPEs) and a management processing element (MPE) (Qiao et al.,
374 2017). To make the most of the computing resources of the Sunway TaihuLight, we



375 generate kernel functions for the MPE, which is responsible for the thread control, and
376 CPE, which performs the computations. The kernel functions are fully optimized with
377 several code optimization techniques (Pugh, 1991) such as loop tiling, loop aligning,
378 single-instruction multiple-date (SIMD) vectorization, and function inline. In addition,
379 due to the high memory access latency of CPEs, we accelerate data access by providing
380 instructions for direct memory access in the kernel to transfer data between the main
381 memory and local memory (Fu et al., 2017).

382

383 **4. Implementation of GOMO**

384 In this section, we introduce how to implement a practical ocean model using
385 OpenArray. The most important step is to derive the primitive discrete governing
386 equations in operator expression form, then the following work will be completed by
387 OpenArray.

388

389 The fundamental equations of GOMO are derived from POM. GOMO features a
390 bottom-following, free-surface, staggered Arakawa C grid. To effectively evolve the
391 rapid surface fluctuations, GOMO uses the mode-splitting algorithm to address the fast
392 propagating surface gravity waves and slow propagating internal waves in barotropic
393 (external) and baroclinic (internal) modes, respectively. The details of the continuous
394 governing equations, the corresponding operator expression form and the descriptions
395 of all the variables used in GOMO are listed in the Appendix A, Appendix B, and
396 Appendix C, respectively.

397

398 Figure 8 shows the basic flow diagram of GOMO. At the beginning of the workflow,
399 we initialize OpenArray to make all operators suitable for GOMO. After loading the
400 initial values and the model parameters, the distance information is input into the
401 differential operators through grid binding. In the external mode, the main consumption
402 is computing the 2-dimensional sea surface elevation η and column-averaged velocity
403 (Ua, Va). In the internal mode, 3-dimensional array computations predominate in order



404 to calculate baroclinic motions (U, V, W), tracers (T, S, ρ), and turbulence closure sub-
405 model (q^2, q^2l) (Mellor and Yamada, 1982), where (U, V, W) are the velocity fields in
406 the x, y and σ directions, (T, S, ρ) are the potential temperature, the salinity and the
407 density. ($q^2/2, q^2l/2$) are the turbulence kinetic energy and production of turbulence
408 kinetic energy with turbulence length scale.

409

410 Because the complicated parallel optimization and tuning processes are decoupled from
411 the ocean modelling, we completely implemented GOMO based on OpenArray in only
412 4 weeks, whereas implementation may take several months or even longer when using
413 the MPI or CUDA library.

414

415 In comparison with the existing POM and its multiple variations, to name a few, Stony
416 Brook Parallel Ocean Model (sbPOM), mpiPOM and POMgpu, GOMO has less code
417 but is more powerful in terms of compatibility. As shown in Table 3, the serial version
418 of POM (POM2k) contains 3521 lines of code. sbPOM and mpiPOM are parallelized
419 using MPI, while POMgpu is based on MPI and CUDA-C. The codes of sbPOM,
420 mpiPOM and POMgpu are extended to 4801, 9680 and 30443 lines. In contrast, the
421 code of GOMO is decreased to 1860 lines. Moreover, GOMO completes the same
422 function as the other approaches while using the least amount of code (Table 4).

423

424 In addition, poor portability considerably restricts the use of advanced hardware in
425 oceanography. With the advantages of OpenArray, GOMO is adaptable to different
426 hardware architectures, such as the Sunway processor. The modellers do not need to
427 modify any code when changing platforms, completely eliminating the heavy burden
428 of transmitting code. As computing platforms become increasingly diverse and
429 complex, GOMO becomes more powerful and attractive than the machine-dependent
430 models.

431



432 **5. Experimental results**

433 In this section, we first evaluate the basic performance of OpenArray using benchmark
434 tests on a single CPU platform. After checking the correctness of GOMO through an
435 ideal seamount test case, we use GOMO to further test the scalability and efficiency of
436 OpenArray.

437

438 **5.1 Benchmark testing**

439 We choose four typical PDEs and their implementations from Rodinia v3.1, which is a
440 benchmark suite for heterogeneous computing (Che et al., 2009), as the original version.
441 For comparison, we re-implement these four PDEs using OpenArray. As shown in
442 Table 5, the 2D continuity equation is used to solve sea surface height, and its
443 continuous form is shown in Eq. (1). The 2D heat diffusion equation is a parabolic PDE
444 that describes the distribution of heat over time in a given region. Hotspot is a thermal
445 simulation used for estimating processor temperature on structured grids (Che et al.,
446 2009; Huang et al., 2006). We tested one 2-dimensional case (Hotspot2D) and one 3-
447 dimensional case (Hotspot3D) of this program. The average runtime for 100 iterations
448 is taken as the performance metric. All tests are executed on a single workstation with
449 an Intel Xeon E5-2650 CPU. The experimental results show that the performance of
450 OpenArray versions is comparable to the original versions.

451

452 **5.2 Validation tests of GOMO**

453 The seamount problem proposed by Beckman and Haidvogel is a widely used ideal test
454 case for regional ocean models (Beckmann and Haidvogel, 1993). It is a stratified
455 Taylor column problem, which simulates the flow over an isolated seamount with a
456 constant salinity and a reference vertical temperature stratification. An eastward
457 horizontal current of 0.1 m/s is added at model initialization. The southern and northern
458 boundaries are closed. If the Rossby number is small, an obvious anticyclonic
459 circulation is trapped by the mount in the deep water.

460



461 Using the seamount test case, we compare GOMO and sbPOM results. The
462 configurations of both models are exactly the same. Figure 9 shows that GOMO and
463 sbPOM both capture the anticyclonic circulation at 3500 metres depth. The shaded plot
464 shows the surface elevation, and the array plot shows the current at 3500 metres. Figure
465 9(a), 9(b), and 9(c) are the results of GOMO, sbPOM, and the difference (GOMO-
466 sbPOM), respectively. The differences in the surface elevation and deep currents
467 between the two models are negligible (Fig. 9(c)).

468

469 **5.3 The weak and strong scalability of GOMO**

470 The seamount test case is used to compare the performance of sbPOM and GOMO in
471 a parallel environment. Figure 10(a) shows the result of a strong scaling evaluation, in
472 which the model size is fixed at $2048 \times 2048 \times 50$. The dashed line indicates the ideal
473 speedup. For the largest parallelisms with 4096 processes, GOMO and sbPOM achieve
474 91% and 92% parallel efficiency, respectively. Figure 10(b) shows the weak scalability
475 of sbPOM and GOMO. In the weak scaling test, the model size for each process is fixed
476 at $128 \times 128 \times 50$, and the number of processes is gradually increased from 16 to 4096.
477 Taking the performance of 16 processes as a baseline, we determine that the parallel
478 efficiencies of GOMO and sbPOM using 4096 processes are 99.0% and 99.2%,
479 respectively.

480

481 **5.4 Testing on the Sunway platform**

482 The strong scalability of GOMO is also tested on the Sunway TaihuLight
483 supercomputer. Supposing that the baseline is the runtime of GOMO at 10000 cores
484 with a grid size of $4096 \times 4096 \times 50$, the parallel efficiency of GOMO can still reach 85%
485 at 150000 cores, as shown in Fig. 11. However, we notice that the scalability declines
486 sharply when the number of cores exceeds 150000. There are two reasons leading to
487 this decline. First, the block size assigned to each core decreases as the number of cores
488 increases, causing more communication during boundary region updating. Second,
489 some processes cannot be accelerated even though more computing resources are



490 available; for example, the time spent on creating the computation graph, generating
491 the fusion kernels, and compiling the JIT cannot be reduced. In a sense, OpenArray
492 performs better when processing large-scale data, and GOMO is more suitable for high-
493 resolution scenarios. In the future, we will further optimize the communication and
494 graph-creating modules to improve the efficiency for large-scale cores.

495

496 **6. Conclusion**

497 We designed a simple computing library (OpenArray) to decouple ocean modelling and
498 parallel computing. OpenArray provides twelve basic operators that are abstracted from
499 PDEs and extended to ocean model governing equations. These operators feature user-
500 friendly interfaces and an implicit parallelization ability. Meanwhile, some state-of-art
501 optimization mechanisms, including computation graphing, kernel fusion, dynamic
502 source code generation and JIT compiling, are applied to boost the performance. The
503 experimental results prove that the performance of a program using OpenArray is
504 comparable to that of well-designed programs using Fortran. Based on OpenArray, we
505 implement a practical ocean model (GOMO) with a high productivity, an enhanced
506 readability and an excellent scalable performance. Moreover, GOMO shows high
507 scalability on the Sunway platform. Although more realistic tests are
508 needed, OpenArray may signal the beginning of a new frontier in future ocean
509 modelling through ingesting basic operators and cutting-edge computing techniques.

510

511 *Code availability.* OpenArray v1.0 is available at
512 https://github.com/hxmhuang/OpenArray_CXX. GOMO is available at
513 <https://github.com/hxmhuang/GOMO>.

514

515 **Appendix A: Continuous governing equations**

516 The equations governing the baroclinic (internal) mode in GOMO are the 3-
517 dimensional hydrostatic primitive equations.



$$518 \quad \frac{\partial \eta}{\partial t} + \frac{\partial UD}{\partial x} + \frac{\partial VD}{\partial y} + \frac{\partial W}{\partial \sigma} = 0 \quad (A1)$$

$$519 \quad \frac{\partial UD}{\partial t} + \frac{\partial U^2 D}{\partial x} + \frac{\partial UV D}{\partial y} + \frac{\partial UW}{\partial \sigma} - fVD + gD \frac{\partial \eta}{\partial x} = \frac{\partial}{\partial \sigma} \left(\frac{K_M}{D} \frac{\partial U}{\partial \sigma} \right) +$$

$$520 \quad \frac{gD^2}{\rho_0} \frac{\partial}{\partial x} \int_{\sigma}^0 \rho d\sigma' - \frac{gD}{\rho_0} \frac{\partial D}{\partial x} \int_{\sigma}^0 \sigma' \frac{\partial \rho}{\partial \sigma'} d\sigma' + F_u \quad (A2)$$

$$521 \quad \frac{\partial VD}{\partial t} + \frac{\partial UV D}{\partial x} + \frac{\partial V^2 D}{\partial y} + \frac{\partial VW}{\partial \sigma} + fUD + gD \frac{\partial \eta}{\partial y} = \frac{\partial}{\partial \sigma} \left(\frac{K_M}{D} \frac{\partial V}{\partial \sigma} \right) +$$

$$522 \quad \frac{gD^2}{\rho_0} \frac{\partial}{\partial y} \int_{\sigma}^0 \rho d\sigma' - \frac{gD}{\rho_0} \frac{\partial D}{\partial y} \int_{\sigma}^0 \sigma' \frac{\partial \rho}{\partial \sigma'} d\sigma' + F_v \quad (A3)$$

$$523 \quad \frac{\partial TD}{\partial t} + \frac{\partial TUD}{\partial x} + \frac{\partial TVD}{\partial y} + \frac{\partial TW}{\partial \sigma} = \frac{\partial}{\partial \sigma} \left(K_H \frac{\partial T}{\partial \sigma} \right) + F_T + \frac{\partial R}{\partial \sigma} \quad (A4)$$

$$524 \quad \frac{\partial SD}{\partial t} + \frac{\partial SUD}{\partial x} + \frac{\partial SVD}{\partial y} + \frac{\partial SW}{\partial \sigma} = \frac{\partial}{\partial \sigma} \left(K_H \frac{\partial S}{\partial \sigma} \right) + F_S \quad (A5)$$

$$525 \quad \rho = \rho(T, S, p) \quad (A6)$$

$$526 \quad \frac{\partial q^2 D}{\partial t} + \frac{\partial Uq^2 D}{\partial x} + \frac{\partial Vq^2 D}{\partial y} + \frac{\partial Wq^2}{\partial \sigma} = \frac{\partial}{\partial \sigma} \left(\frac{K_q}{D} \frac{\partial q^2}{\partial \sigma} \right) + \frac{2K_M}{D} \left[\left(\frac{\partial U}{\partial \sigma} \right)^2 + \left(\frac{\partial V}{\partial \sigma} \right)^2 \right] +$$

$$527 \quad \frac{2g}{\rho_0} K_H \frac{\partial \rho}{\partial \sigma} - \frac{2Dq^3}{B_1 l} + F_{q^2} \quad (A7)$$

$$528 \quad \frac{\partial q^2 l D}{\partial t} + \frac{\partial Uq^2 l D}{\partial x} + \frac{\partial Vq^2 l D}{\partial y} + \frac{\partial Wq^2 l}{\partial \sigma} = \frac{\partial}{\partial \sigma} \left(\frac{K_q}{D} \frac{\partial q^2 l}{\partial \sigma} \right) + E_1 l \left\{ \frac{K_M}{D} \left[\left(\frac{\partial U}{\partial \sigma} \right)^2 + \right. \right.$$

$$529 \quad \left. \left(\frac{\partial V}{\partial \sigma} \right)^2 \right] + \frac{gE_3}{\rho_0} K_H \frac{\partial \rho}{\partial \sigma} \right\} \tilde{W} - \frac{Dq^3}{B_1} + F_{q^2 l} \quad (A8)$$

530

531 Where F_u , F_v , F_{q^2} , and $F_{q^2 l}$ are horizontal kinematic viscosity terms of u , v , q^2 , and

532 $q^2 l$, respectively. F_T and F_S are horizontal diffusion terms of T and S respectively. \tilde{W}

533 is the wall proximity function.

$$534 \quad F_u = \frac{\partial}{\partial x} (2A_M D \frac{\partial U}{\partial x}) + \frac{\partial}{\partial y} \left[A_M D \left(\frac{\partial U}{\partial y} + \frac{\partial V}{\partial x} \right) \right] \quad (A9)$$

$$535 \quad F_v = \frac{\partial}{\partial y} (2A_M D \frac{\partial V}{\partial y}) + \frac{\partial}{\partial x} \left[A_M D \left(\frac{\partial U}{\partial y} + \frac{\partial V}{\partial x} \right) \right] \quad (A10)$$

$$536 \quad F_T = \frac{\partial}{\partial x} (A_H H \frac{\partial T}{\partial x}) + \frac{\partial}{\partial y} (A_H H \frac{\partial T}{\partial y}) \quad (A11)$$

$$537 \quad F_S = \frac{\partial}{\partial x} (A_H H \frac{\partial S}{\partial x}) + \frac{\partial}{\partial y} (A_H H \frac{\partial S}{\partial y}) \quad (A12)$$

$$538 \quad F_{q^2} = \frac{\partial}{\partial x} (A_M H \frac{\partial q^2}{\partial x}) + \frac{\partial}{\partial y} (A_M H \frac{\partial q^2}{\partial y}) \quad (A13)$$

$$539 \quad F_{q^2 l} = \frac{\partial}{\partial x} (A_M H \frac{\partial q^2 l}{\partial x}) + \frac{\partial}{\partial y} (A_M H \frac{\partial q^2 l}{\partial y}) \quad (A14)$$

$$540 \quad \tilde{W} = 1 + \frac{E_2 l}{\kappa} \left(\frac{1}{\eta - z} + \frac{1}{H - z} \right) \quad (A15)$$



541 The equations governing the barotropic (external) mode in GOMO are obtained by
 542 vertically integrating the baroclinic equations.

$$543 \quad \frac{\partial \eta}{\partial t} + \frac{\partial U_{AD}}{\partial x} + \frac{\partial V_{AD}}{\partial y} = 0 \quad (\text{A16})$$

$$544 \quad \frac{\partial U_{AD}}{\partial t} + \frac{\partial (U_A)^2 D}{\partial x} + \frac{\partial U_A V_{AD}}{\partial y} - f V_A D + g D \frac{\partial \eta}{\partial x} = \tilde{F}_{u_a} - wu(0) +$$

$$545 \quad wu(-1) - \frac{gD}{\rho_0} \int_{-1}^0 \int_{\sigma} \left[D \frac{\partial \rho}{\partial x} - \frac{\partial D}{\partial x} \sigma' \frac{\partial \rho}{\partial \sigma} \right] d\sigma' d\sigma + G_{u_a} \quad (\text{A17})$$

$$546 \quad \frac{\partial V_{AD}}{\partial t} + \frac{\partial U_A V_{AD}}{\partial y} + \frac{\partial (V_A)^2 D}{\partial y} + f U_A D + g D \frac{\partial \eta}{\partial y} = \tilde{F}_{v_a} - wv(0) +$$

$$547 \quad wv(-1) - \frac{gD}{\rho_0} \int_{-1}^0 \int_{\sigma} \left[D \frac{\partial \rho}{\partial y} - \frac{\partial D}{\partial y} \sigma' \frac{\partial \rho}{\partial \sigma} \right] d\sigma' d\sigma + G_{v_a} \quad (\text{A18})$$

548

549 Where \tilde{F}_{u_a} and \tilde{F}_{v_a} are the horizontal kinematic viscosity terms of U_A and V_A
 550 respectively. G_{u_a} and G_{v_a} are the dispersion terms of U_A and V_A respectively. The
 551 subscript 'A' denotes vertical integration.

552

$$553 \quad \tilde{F}_{u_a} = \frac{\partial}{\partial x} \left[2H(AA_M) \frac{\partial U_A}{\partial x} \right] + \frac{\partial}{\partial y} \left[H(AA_M) \left(\frac{\partial U_A}{\partial y} + \frac{\partial V_A}{\partial x} \right) \right] \quad (\text{A19})$$

$$554 \quad \tilde{F}_{v_a} = \frac{\partial}{\partial y} \left[2H(AA_M) \frac{\partial V_A}{\partial y} \right] + \frac{\partial}{\partial x} \left[H(AA_M) \left(\frac{\partial U_A}{\partial y} + \frac{\partial V_A}{\partial x} \right) \right] \quad (\text{A20})$$

$$555 \quad G_{u_a} = \frac{\partial^2 (U_A)^2 D}{\partial x^2} + \frac{\partial^2 U_A V_{AD}}{\partial x \partial y} - \tilde{F}_{u_a} - \frac{\partial^2 (U^2)_{AD}}{\partial x^2} - \frac{\partial^2 (UV)_{AD}}{\partial y^2} + (F_u)_A \quad (\text{A21})$$

$$556 \quad G_{v_a} = \frac{\partial^2 U_A V_{AD}}{\partial x \partial y} + \frac{\partial^2 (V_A)^2 D}{\partial y^2} - \tilde{F}_{v_a} - \frac{\partial^2 (UV)_{AD}}{\partial x^2} - \frac{\partial^2 (V^2)_{AD}}{\partial y^2} + (F_v)_A \quad (\text{A22})$$

$$557 \quad U_A = \int_{-1}^0 U d\sigma \quad (\text{A23})$$

$$558 \quad V_A = \int_{-1}^0 V d\sigma \quad (\text{A24})$$

$$559 \quad (U^2)_A = \int_{-1}^0 U^2 d\sigma \quad (\text{A25})$$

$$560 \quad (UV)_A = \int_{-1}^0 UV d\sigma \quad (\text{A26})$$

$$561 \quad (V^2)_A = \int_{-1}^0 V^2 d\sigma \quad (\text{A27})$$

$$562 \quad (F_u)_A = \int_{-1}^0 F_u d\sigma \quad (\text{A28})$$

$$563 \quad (F_v)_A = \int_{-1}^0 F_v d\sigma \quad (\text{A29})$$



$$564 \quad AA_M = \int_{-1}^0 (A_M) d\sigma \quad (A30)$$

565

566 Appendix B: Discrete governing equations

567 The discrete governing equations of baroclinic (internal) mode expressed by operators
 568 are shown as below:

$$569 \quad \frac{\eta^{t+1} - \eta^{t-1}}{2dti} + \delta_f^x (\overline{D_b^x} U) + \delta_f^y (\overline{D_b^y} V) + \delta_f^z (W) = 0 \quad (B1)$$

$$570 \quad \frac{(\overline{D_b^x} U)^{t+1} - (\overline{D_b^x} U)^{t-1}}{2dti} + \delta_b^x \left[\overline{(\overline{D_b^x} U)_f \overline{U}_f^x} \right] + \delta_f^y \left[\overline{(\overline{D_b^y} V)_b \overline{U}_b^y} \right] +$$

$$571 \quad \delta_f^z \left[\overline{(\overline{W}_b^x \overline{U}_b^z)} - \overline{(\overline{f \overline{V}_f^y} D)_b} - \overline{(\overline{f \overline{V}_f^y} D)_b} + g \overline{D_b^x} \delta_b^x (\eta) \right] = \delta_b^z \left[\frac{\overline{K_{Mb}^x}}{(\overline{D_b^x})^{t+1}} \delta_f^z (U^{t+1}) \right] +$$

$$572 \quad \frac{g (\overline{D_b^x})^2}{\rho_0} \int_{\sigma}^0 \left[\delta_b^x (\overline{\rho_b^z}) - \frac{\sigma}{\overline{D_b^x}} \delta_b^x (\overline{\rho_b^z}) \right] d\sigma' + F_u \quad (B2)$$

$$573 \quad \frac{(\overline{D_b^y} V)^{t+1} - (\overline{D_b^y} V)^{t-1}}{2dti} + \delta_f^x \left[\overline{(\overline{D_b^x} U)_b \overline{V}_b^x} \right] + \delta_b^y \left[\overline{(\overline{D_b^y} V)_f \overline{V}_f^y} \right] +$$

$$574 \quad \delta_f^z \left[\overline{(\overline{W}_b^y \overline{V}_b^z)} + \overline{(\overline{f \overline{U}_f^x} D)_b} + \overline{(\overline{f \overline{U}_f^x} D)_b} + g \overline{D_b^y} \delta_b^y (\eta) \right] = \delta_b^z \left[\frac{\overline{K_{Mb}^y}}{(\overline{D_b^y})^{t+1}} \delta_f^z (V^{t+1}) \right] +$$

$$575 \quad \frac{g (\overline{D_b^y})^2}{\rho_0} \int_{\sigma}^0 \left[\delta_b^y (\overline{\rho_b^z}) - \frac{\sigma}{\overline{D_b^y}} \delta_b^y (\overline{\rho_b^z}) \right] d\sigma' + F_v \quad (B3)$$

$$576 \quad \frac{(TD)^{t+1} - (TD)^{t-1}}{2dti} + \delta_f^x (\overline{T_b^x} U \overline{D_b^x}) + \delta_f^y (\overline{T_b^y} V \overline{D_b^y}) + \delta_f^z (\overline{T_b^z} W) =$$

$$577 \quad \delta_b^z \left[\frac{K_H}{D^{t+1}} \delta_f^z (T^{t+1}) \right] + F_T + \delta_f^z R \quad (B4)$$

$$578 \quad \frac{(SD)^{t+1} - (SD)^{t-1}}{2dti} + \delta_f^x (\overline{S_b^x} U \overline{D_b^x}) + \delta_f^y (\overline{S_b^y} V \overline{D_b^y}) + \delta_f^z (\overline{S_b^z} W) =$$

$$579 \quad \delta_b^z \left[\frac{K_H}{D^{t+1}} \delta_f^z (S^{t+1}) \right] + F_S \quad (B5)$$

$$580 \quad \rho = \rho(T, S, p) \quad (B6)$$

$$581 \quad \frac{(q^2 D)^{t+1} - (q^2 D)^{t-1}}{2dti} + \delta_f^x (\overline{U_b^z} \overline{q_b^2} \overline{D_b^x}) + \delta_f^y (\overline{V_b^z} \overline{q_b^2} \overline{D_b^y}) +$$

$$582 \quad \delta_f^z \left[\overline{(\overline{W} q^2)_b} \right] = \delta_b^z \left[\frac{\overline{K_{qf}^z}}{D^{t+1}} \delta_f^z (q^2)^{t+1} \right] + \frac{2K_M}{D} \left\{ \left[\delta_b^z (\overline{U}_f^x) \right]^2 + \left[\delta_b^z (\overline{V}_f^y) \right]^2 \right\} +$$

$$583 \quad \frac{2g}{\rho_0} K_H \delta_b^z (\rho) - \frac{2Dq^3}{B_1 l} + F_{q^2} \quad (B7)$$

$$584 \quad \frac{(q^2 ID)^{t+1} - (q^2 ID)^{t-1}}{2dti} + \delta_f^x (\overline{U_b^z} \overline{q_b^2} \overline{l_b} \overline{D_b^x}) + \delta_f^y (\overline{V_b^z} \overline{q_b^2} \overline{l_b} \overline{D_b^y}) +$$



$$\begin{aligned}
 585 \quad \delta_f^z \overline{(Wq^2)_b^z} &= \delta_b^z \left[\frac{\overline{K_{qf}^z}}{D^{t+1}} \delta_f^z (q^2 l)^{t+1} \right] + lE_1 \frac{K_M}{D} \left\{ \left[\delta_b^z \overline{(U_f^x)} \right]^2 + \left[\delta_b^z \overline{(V_f^y)} \right]^2 \right\} \tilde{W} + \\
 586 \quad \frac{lE_1 E_3 g}{\rho_0} K_H \delta_b^z (\rho) \tilde{W} &- \frac{Dq^3}{B_1} + F_{q^2 l} \quad (B8)
 \end{aligned}$$

587

588 Where F_u , F_v , F_{q^2} , and $F_{q^2 l}$ are horizontal kinematic viscosity terms of u , v , q^2 , and

589 $q^2 l$, respectively. F_T and F_S are horizontal diffusion terms of T and S respectively.

$$590 \quad F_u = \delta_b^x \left[2A_M D \delta_f^x (U^{t-1}) \right] + \delta_f^y \left\{ \overline{(A_{Mb}^x)}_b \overline{(D_b^x)}_b \left[\delta_b^x (V)^{t-1} + \delta_b^y (U)^{t-1} \right] \right\} \quad (B9)$$

$$591 \quad F_v = \delta_b^y \left[2A_M D \delta_f^y (V^{t-1}) \right] + \delta_f^x \left\{ \overline{(A_{Mb}^y)}_b \overline{(D_b^y)}_b \left[\delta_b^x (V)^{t-1} + \delta_b^y (U)^{t-1} \right] \right\} \quad (B10)$$

$$592 \quad F_T = \delta_f^x \left[\overline{(A_{Hb}^x)}_b \overline{(H_b^x)}_b \delta_b^x (T^{t-1}) \right] + \delta_f^y \left[\overline{(A_{Hb}^y)}_b \overline{(H_b^y)}_b \delta_b^y (T^{t-1}) \right] \quad (B11)$$

$$593 \quad F_S = \delta_f^x \left[\overline{(A_{Hb}^x)}_b \overline{(H_b^x)}_b \delta_b^x (S^{t-1}) \right] + \delta_f^y \left[\overline{(A_{Hb}^y)}_b \overline{(H_b^y)}_b \delta_b^y (S^{t-1}) \right] \quad (B12)$$

$$594 \quad F_{q^2} = \delta_f^x \left[\overline{(A_{Mb}^x)}_b \overline{(H_b^x)}_b \delta_b^x (q^2)^{t-1} \right] + \delta_f^y \left[\overline{(A_{Mb}^y)}_b \overline{(H_b^y)}_b \delta_b^y (q^2)^{t-1} \right] \quad (B13)$$

$$595 \quad F_{q^2 l} = \delta_f^x \left[\overline{(A_{Mb}^x)}_b \overline{(H_b^x)}_b \delta_b^x (q^2 l)^{t-1} \right] + \delta_f^y \left[\overline{(A_{Mb}^y)}_b \overline{(H_b^y)}_b \delta_b^y (q^2 l)^{t-1} \right] \quad (B14)$$

596

597 The discrete governing equations of barotropic (external) mode expressed by operators

598 are shown as below:

$$599 \quad \frac{\eta^{t+1} - \eta^{t-1}}{2dte} + \delta_f^x \overline{(D_b^x)}_b U_A + \delta_f^y \overline{(D_b^y)}_b V_A = 0 \quad (B15)$$

$$600 \quad \frac{\overline{(D_b^x U_A)}_b^{t+1} - \overline{(D_b^x U_A)}_b^{t-1}}{2dte} + \delta_b^x \left[\overline{(D_b^x U_A)}_f (U_A)_f^x \right] + \delta_f^y \left[\overline{(D_b^y V_A)}_b (U_A)_b^y \right] -$$

$$601 \quad \left[\overline{(f_A)}_f \overline{(V_A)}_f^y D \right]_b^x - \left[\overline{(f_A)}_f \overline{(V_A)}_f^y D \right]_b^x + g \overline{(D_b^x)}_b \delta_b^x (\eta) = \delta_b^x \{ 2(AA_M) D \delta_f^x [(U_A)^{t-1}] \} +$$

$$602 \quad \delta_f^y \left\{ \left[\overline{(AA_M)}_b^x \right]_b \overline{(D_b^x)}_b \left[\delta_b^x (V_A) + \delta_b^y (U_A) \right]^{t-1} \right\} + \phi_x \quad (B16)$$

$$603 \quad \frac{\overline{(D_b^y V_A)}_b^{t+1} - \overline{(D_b^y V_A)}_b^{t-1}}{2dte} + \delta_f^x \left[\overline{(D_b^x U_A)}_b (V_A)_b^x \right] + \delta_b^y \left[\overline{(D_b^y V_A)}_f (V_A)_f^y \right] +$$



$$\begin{aligned}
 604 \quad & \overline{[f_A(U_A)_f^x D]}_b^y + \overline{[f(U_A)_f^x D]}_b^y + g\overline{D}_b^y \delta_b^y(\eta) = \delta_b^y \{2(AA_M)D\delta_f^y [(V_A)^{t-1}] \} + \\
 605 \quad & \delta_f^x \left\{ \overline{[(AA_M)_b^x]}_b^y \overline{(\overline{D}_b^x)}_b^y [\delta_b^x(V_A) + \delta_b^y(U_A)]^{t-1} \right\} + \phi_y \quad (B17)
 \end{aligned}$$

606

607 where

$$\begin{aligned}
 608 \quad & \phi_x = -WU(0) + WU(-1) - \frac{g(\overline{D}_b^x)^2}{\rho_0} \int_{-1}^0 \left\{ \left[\int_{\sigma}^0 \delta_b^x(\overline{\rho})_b^z d\sigma' \right] d\sigma \right\} + \\
 609 \quad & \frac{g\overline{D}_b^x \delta_b^x D}{\rho_0} \int_{-1}^0 \left\{ \left[\int_{\sigma}^0 \overline{\sigma}_b^z \delta_b^z(\overline{\rho}_b^x) \right] d\sigma \right\} + G_x \quad (B18)
 \end{aligned}$$

$$\begin{aligned}
 610 \quad & \phi_y = -WV(0) + WV(-1) - \frac{g(\overline{D}_b^y)^2}{\rho_0} \int_{-1}^0 \left\{ \left[\int_{\sigma}^0 \delta_b^y(\overline{\rho})_b^z d\sigma' \right] d\sigma \right\} + \\
 611 \quad & \frac{g\overline{D}_b^y \delta_b^y D}{\rho_0} \int_{-1}^0 \left\{ \left[\int_{\sigma}^0 \overline{\sigma}_b^z \delta_b^z(\overline{\rho}_b^y) \right] d\sigma \right\} + G_y \quad (B19)
 \end{aligned}$$

612

613



614 **Appendix C: Descriptions of symbols**

615 The description of each symbol in the governing equations is list as below:

616 Table C1. Descriptions of symbols

Symbol	Description
η	Free surface elevation
H	Bottom topography
ua, va	Vertical average velocity in x, y direction, respectively
U, V, W	Velocity in x, y, σ direction, respectively
D	Fluid column depth
f	The Coriolis parameter
g	The gravitational acceleration
ρ_0	Constant density
ρ	Situ density
T	Potential temperature
S	Salinity
R	Surface solar radiation incident
$q^2/2$	Turbulence kinetic energy
l	Turbulence length scale
$q^2l/2$	Production of turbulence kinetic energy and turbulence length scale
dti	Time step of baroclinic mode
dte	Time step of barotropic mode
dx	Grid increment in x direction
dy	Grid increment in y direction
A_M	Horizontal kinematic viscosity
A_H	Horizontal heat diffusivity
K_M	Vertical kinematic viscosity
K_H	Vertical mixing coefficient of heat and salinity
K_q	Vertical mixing coefficient of turbulence kinetic energy



618 *Author contributions.* Xiaomeng Huang, Xing Huang, DW, QW, and SZ designed
619 OpenArray. Xing Huang, MW, YG, and QT implemented and tested GOMO.
620 Xiaomeng Huang and Xing Huang led the writing of this paper with contributions from
621 all other coauthors.

622

623 *Competing interests.* The authors declare that they have no conflict of interest.

624

625 *Acknowledgements.* Xiaomeng Huang is supported by a grant from the State's Key
626 Project of Research and Development Plan (2016YFB0201100) and the National
627 Natural Science Foundation of China (41776010). Xing Huang is supported by a grant
628 from the State's Key Project of Research and Development Plan (2018YFB0505000).
629 Shixun Zhang is supported by a grant from the State's Key Project of Research and
630 Development Plan (2017YFC1502200) and Qingdao National Laboratory for Marine
631 Science and Technology (QNL2016ORP0108). Zhenya Song is supported by
632 National Natural Science Foundation of China (U1806205) and AoShan Talents
633 Cultivation Excellent Scholar Program Supported by Qingdao National Laboratory for
634 Marine Science and Technology (2017ASTCP-ES04).

635

636 **References**

637 Abadi, M., Barham, P., Chen, J., Chen, Z., Davis, A., Dean, J., Devin, M., Ghemawat,
638 S., Irving, G., Isard, M., Kudlur, M., Levenberg, J., Monga, R., Moore, S., Murray,
639 D. G., Steiner, B., Tucker, P., Vasudevan, V., Warden, P., Wicke, M., Yu, Y. and
640 Zheng, X.: TensorFlow: A System for Large-Scale Machine Learning, in 12th
641 {USENIX} Symposium on Operating Systems Design and Implementation ({OSDI}
642 16), pp. 265–283, {USENIX} Association, Savannah, GA. [online] Available from:
643 <https://www.usenix.org/conference/osdi16/technical-sessions/presentation/abadi>,
644 2016.

645 Adcroft, A., Campin, J.-M., Dutkiewicz, S., Constantinos, E., Ferreira, D., Forget, G.,
646 Fox-Kemper, B., Heimbach, P., Hill, C., Hill, E., Hill, H., Jahn, O., Losch, M.,



- 647 Marshall, J., Maze, G., Menemenlis, D. and Molod, A.: MITgcm User Manual,
648 Intern. Doc., doi:1721.1/117188, 2017.
- 649 Alexander, K. and Easterbrook, S. M.: The software architecture of climate models: A
650 graphical comparison of CMIP5 and EMICAR5 configurations, Geosci. Model Dev.,
651 8(4), 1221–1232, doi:10.5194/gmd-8-1221-2015, 2015.
- 652 Arakawa, A. and Lamb, V. R.: A Potential Enstrophy and Energy Conserving Scheme
653 for the Shallow Water Equations, Mon. Weather Rev., doi:10.1175/1520-
654 0493(1981)109<0018:APEAEC>2.0.CO;2, 1981.
- 655 Bae, H., Mustafa, D., Lee, J. W., Aurangzeb, Lin, H., Dave, C., Eigenmann, R. and
656 Midkiff, S. P.: The Cetus source-to-source compiler infrastructure: Overview and
657 evaluation, in International Journal of Parallel Programming., 2013.
- 658 Bastien, F., Lamblin, P., Pascanu, R., Bergstra, J., Goodfellow, I. J., Bergeron, A.,
659 Bouchard, N., Warde-Farley, D. and Bengio, Y.: Theano: new features and speed
660 improvements, CoRR, abs/1211.5 [online] Available from:
661 <http://arxiv.org/abs/1211.5590>, 2012.
- 662 Beckmann, A. and Haidvogel, D. B.: Numerical simulation of flow around a tall
663 isolated seamount. Part I: problem formulation and model accuracy, J. Phys.
664 Oceanogr., 23(8), 1736–1753, doi:10.1175/1520-
665 0485(1993)023<1736:NSOFAA>2.0.CO;2, 1993.
- 666 Bloss, A., Hudak, P. and Young, J.: Code optimizations for lazy evaluation, Lisp Symb.
667 Comput., doi:10.1007/BF01806169, 1988.
- 668 Blumberg, A. F. and Mellor, G. L.: A description of a three-dimensional coastal ocean
669 circulation model, (January 1987), 1–16, doi:10.1029/CO004p0001, 1987.
- 670 Bonan, G. B. and Doney, S. C.: Climate, ecosystems, and planetary futures: The
671 challenge to predict life in Earth system models, Science (80-.),
672 doi:10.1126/science.aam8328, 2018.
- 673 Bretherton, C., Balaji, V., Delworth, T. et al: A National Strategy for Advancing
674 Climate Modeling, National Academies Press., 2012.
- 675 Che, S., Boyer, M., Meng, J., Tarjan, D., Sheaffer, J. W., Lee, S. H. and Skadron, K.:



- 676 Rodinia: A benchmark suite for heterogeneous computing, in Proceedings of the
677 2009 IEEE International Symposium on Workload Characterization, IISWC 2009.,
678 2009.
- 679 Chen, C., Liu, H. and Beardsley, R. C.: An unstructured grid, finite-volume, three-
680 dimensional, primitive equations ocean model: Application to coastal ocean and
681 estuaries, *J. Atmos. Ocean. Technol.*, doi:10.1175/1520-
682 0426(2003)020<0159:AUGFVT>2.0.CO;2, 2003.
- 683 Collins, M., Minobe, S., Barreiro, M., Bordoni, S., Kaspi, Y., Kuwano-Yoshida, A.,
684 Keenlyside, N., Manzini, E., O'Reilly, C. H., Sutton, R., Xie, S. P. and Zolina, O.:
685 Challenges and opportunities for improved understanding of regional climate
686 dynamics, *Nat. Clim. Chang.*, 8(2), 101–108, doi:10.1038/s41558-017-0059-8,
687 2018.
- 688 Corliss, G. and Griewank, A.: Operator Overloading as an Enabling Technology for
689 Automatic Differentiation, 1994.
- 690 van Engelen, R. a.: ATMOL: A Domain-Specific Language for Atmospheric Modeling,
691 *J. Comput. Inf. Technol.*, 9(4), 289–303, doi:10.2498/cit.2001.04.02, 2001.
- 692 Fringer, O. B., Gerritsen, M. and Street, R. L.: An unstructured-grid, finite-volume,
693 nonhydrostatic, parallel coastal ocean simulator, *Ocean Model.*,
694 doi:10.1016/j.ocemod.2006.03.006, 2006.
- 695 Fu, H., He, C., Chen, B., Yin, Z., Zhang, Z., Zhang, W., Zhang, T., Xue, W., Liu, W.,
696 Yin, W. and others: 18.9-Pflops nonlinear earthquake simulation on Sunway
697 TaihuLight: enabling depiction of 18-Hz and 8-meter scenarios, in Proceedings of
698 the International Conference for High Performance Computing, Networking,
699 Storage and Analysis., 2017.
- 700 Griffies, S. M.: Elements of the modular ocean model (MOM), GFDL Ocean Gr. Tech.
701 Rep, 7(C), 620, 2012.
- 702 Griffies, S. M., Böning, C., Bryan, F. O., Chassignet, E. P., Gerdes, R., Hasumi, H.,
703 Hirst, A., Treguier, A.-M. and Webb, D.: Developments in ocean climate modelling,
704 *Ocean Model.*, 2(3–4), 123–192, doi:10.1016/S1463-5003(00)00014-7, 2000.



- 705 Gysi, T., Osuna, C., Fuhrer, O., Bianco, M. and Schulthess, T. C.: STELLA: A Domain-
706 specific Tool for Structured Grid Methods in Weather and Climate Models, Proc.
707 Int. Conf. High Perform. Comput. Networking, Storage Anal. - SC '15, 1–12,
708 doi:10.1145/2807591.2807627, 2015.
- 709 Huang, W., Ghosh, S., Velusamy, S., Sankaranarayanan, K., Skadron, K. and Stan, M.
710 R.: HotSpot: A compact thermal modeling methodology for early-stage VLSI design,
711 IEEE Trans. Very Large Scale Integr. Syst., doi:10.1109/TVLSI.2006.876103, 2006.
- 712 Lawrence, B. N., Rezny, M., Budich, R., Bauer, P., Behrens, J., Carter, M., Deconinck,
713 W., Ford, R., Maynard, C., Mullerworth, S., Osuna, C., Porter, A., Serradell, K.,
714 Valcke, S., Wedi, N. and Wilson, S.: Crossing the chasm: How to develop weather
715 and climate models for next generation computers?, Geosci. Model Dev.,
716 doi:10.5194/gmd-11-1799-2018, 2018.
- 717 Levin, J. G., Iskandarani, M. and Haidvogel, D. B.: A nonconforming spectral element
718 ocean model, Int. J. Numer. Methods Fluids, 34(6), 495–525, doi:10.1002/1097-
719 0363(20001130)34:6<495::AID-FLD68>3.0.CO;2-K, 2000.
- 720 Lidman, J., Quinlan, D. J., Liao, C. and McKee, S. A.: ROSE::FTTransform - A source-
721 to-source translation framework for exascale fault-tolerance research, Proc. Int.
722 Conf. Dependable Syst. Networks, (June), doi:10.1109/DSNW.2012.6264672, 2012.
- 723 Luetlich, R. A., Westerink, J. J. and Scheffner, N.: ADCIRC: an advanced three-
724 dimensional circulation model for shelves coasts and estuaries, report 1: theory and
725 methodology of ADCIRC-2DDI and ADCIRC-3DL., 1992.
- 726 Mellor, G. L. and Yamada, T.: Development of a turbulence closure model for
727 geophysical fluid problems, Rev. Geophys., doi:10.1029/RG020i004p00851, 1982.
- 728 Naumann, U., Utke, J., Heimbach, P., Hill, C., Ozyurt, D., Wunsch, C., Fagan, M.,
729 Tallent, N. and Strout, M.: Adjoint code by source transformation with OpenAD/F,
730 Eur. Conf. Comput. Fluid Dyn. ECCOMAS CFD 2006, (September 2014), ~, 2006.
- 731 Pugh, W.: Uniform Techniques for Loop Optimization, in Proceedings of the 5th
732 International Conference on Supercomputing, pp. 341–352, ACM, New York, NY,
733 USA., 1991.



- 734 Qiao, F., Zhao, W., Yin, X., Huang, X., Liu, X., Shu, Q., Wang, G., Song, Z., Li, X.,
735 Liu, H., Yang, G. and Yuan, Y.: A Highly Effective Global Surface Wave Numerical
736 Simulation with Ultra-High Resolution, in International Conference for High
737 Performance Computing, Networking, Storage and Analysis, SC., 2017.
- 738 Reynolds, J. C.: Theories of Programming Languages, Cambridge University Press,
739 New York, NY, USA., 1999.
- 740 Shchepetkin, A. F. and McWilliams, J. C.: The regional oceanic modeling system
741 (ROMS): A split-explicit, free-surface, topography-following-coordinate oceanic
742 model, *Ocean Model.*, doi:10.1016/j.ocemod.2004.08.002, 2005.
- 743 Smith, R., Jones, P., Briegleb, B., Bryan, F., Danabasoglu, G., Dennis, J., Dukowicz,
744 J., Eden, C., Fox-Kemper, B., Gent, P., Hecht, M., Jayne, S., Jochum, M., Large,
745 W., Lindsay, K., Maltrud, M., Norton, N., Peacock, S., Vertenstein, M. and Yeager,
746 S.: The Parallel Ocean Program (POP) reference manual: Ocean component of the
747 Community Climate System Model (CCSM), Los Alamos Natl. Lab. Tech. Rep.
748 LAUR-10-01853, 141, 1–141 [online] Available from: [www.cesm.ucar.edu/models](http://www.cesm.ucar.edu/models/cesm1.0/pop2/doc/sci/POPRefManual.pdf)
749 [/cesm1.0/pop2/doc/sci/POPRefManual.pdf](http://www.cesm.ucar.edu/models/cesm1.0/pop2/doc/sci/POPRefManual.pdf), 2010.
- 750 Suganuma, T. and Yasue, T.: Design and evaluation of dynamic optimizations for a
751 Java just-in-time compiler, *ACM Trans. ...*, doi:10.1145/1075382.1075386, 2005.
- 752 Taylor, K. E., Stouffer, R. J. and Meehl, G. A.: An overview of CMIP5 and the
753 experiment design, *Bull. Am. Meteorol. Soc.*, 93(4), 485–498, doi:10.1175/BAMS-
754 D-11-00094.1, 2012.
- 755 Torres, R., Linardakis, L., Kunkel, J. and Ludwig, T.: ICON DSL: A Domain-Specific
756 Language for climate modeling, *Sc13.Supercomputing.Org* [online] Available from:
757 <http://sc13.supercomputing.org/sites/default/files/WorkshopsArchive/pdfs/wp127s>
758 [1.pdf](http://sc13.supercomputing.org/sites/default/files/WorkshopsArchive/pdfs/wp127s), 2013.
- 759 Utke, J., Naumann, U., Fagan, M., Tallent, N., Strout, M., Heimbach, P., Hill, C. and
760 Wunsch, C.: OpenAD/F: A Modular Open-Source Tool for Automatic
761 Differentiation of Fortran Codes, *ACM Trans. Math. Softw.*, 34(4), 18:1-18:36,
762 doi:10.1145/1377596.1377598, 2008.



763 Walther, A., Griewank, A. and Vogel, O.: ADOL-C: Automatic Differentiation Using

764 Operator Overloading in C++, PAMM, doi:10.1002/pamm.200310011, 2003.

765 Xu, S., Huang, X., Oey, L. Y., Xu, F., Fu, H., Zhang, Y. and Yang, G.: POM.GPU-v1.0:

766 A GPU-based princeton ocean model, Geosci. Model Dev., doi:10.5194/gmd-8-

767 2815-2015, 2015.

768

769



770 **Tables**

771 **Table 1. Definitions of the twelve basic operators**

Notations	Discrete Form	Basic Operator
\overline{var}_f^x	$[var(i,j,k) + var(i+1,j,k)] / 2$	AXF
\overline{var}_b^x	$[var(i,j,k) + var(i-1,j,k)] / 2$	AXB
\overline{var}_f^y	$[var(i,j,k) + var(i,j+1,k)] / 2$	AYF
\overline{var}_b^y	$[var(i,j,k) + var(i,j-1,k)] / 2$	AYB
\overline{var}_f^z	$[var(i,j,k) + var(i,j,k+1)] / 2$	AZF
\overline{var}_b^z	$[var(i,j,k) + var(i,j,k-1)] / 2$	AZB
$\delta_f^x(var)$	$[var(i+1,j,k) - var(i,j,k)] / dx(i,j)$	DXF
$\delta_b^x(var)$	$[var(i,j,k) - var(i-1,j,k)] / dx(i-1,j)$	DXB
$\delta_f^y(var)$	$[var(i,j+1,k) - var(i,j,k)] / dy(i,j)$	DYF
$\delta_b^y(var)$	$[var(i,j,k) - var(i,j-1,k)] / dy(i,j-1)$	DYB
$\delta_f^z(var)$	$[var(i,j,k+1) - var(i,j,k)] / dz(k)$	DZF
$\delta_b^z(var)$	$[var(i,j,k) - var(i,j,k-1)] / dz(k-1)$	DZB

772

773



774

Table 2 The jumping rules of an operator acting on an *Array*

The initial position of <i>var</i>	The position of $[A D]X[F B]$ (<i>var</i>)	The position of $[A D]Y[F B]$ (<i>var</i>)	The position of $[A D]Z[F B]$ (<i>var</i>)
0	1	2	4
1	0	3	5
2	3	0	6
3	2	1	7
4	5	6	0
5	4	7	1
6	7	4	2
7	6	5	3

775

776



777

Table 3. Comparing GOMO with several variations of the POM

Model	Lines of code	Method	Computing Platforms
POM2k	3521	Serial	CPU
sbPOM	4801	MPI	CPU
mpiPOM	9685	MPI	CPU
POMgpu	30443	MPI + CUDA	GPU
GOMO	1860	OpenArray	CPU, Sunway

778

779



780

Table. 4. Comparison of the amount of code for different functions

Functions	Lines of code		
	POM2k	sbPOM	GOMO
Solve for η	16	72	1
Solve for Ua	75	183	11
Solve for Va	75	183	11
Solve for W	36	90	3
Solve for q^2 and q^2l	318	854	162
Solve for T or S	178	234	71
Solve for U	118	230	50
Solve for V	118	230	50

781

782



783

Table 5. Four benchmark tests

Benchmark	Dimensions	Grid Size	OpenArray version (seconds)	Original version(seconds)
Continuity equation	2D	8192×8192	7.22	7.10
Heat diffusion equation	2D	8192×8192	6.20	6.34
Hotspot2D	2D	8192×8192	11.37	11.21
Hotspot3D	3D	512×512×8	0.96	1.01

784

785



786 **Figures**

\$ 1) 2D continuous equation

$$\eta_{t+1} = \eta_{t-1} - 2 * dt * (\delta_x^y (\bar{D}_b^x * U) + \delta_y^x (\bar{D}_b^y * V))$$

\$ 2) The code constructed by operators

$$elf = elb - 2 * dt * (DXF(AXB(D)*U) + DYF(AYB(D)*V))$$

\$ 3) The pseudo-code

```
exchange2d_mpi(u,im,jm)
exchange2d_mpi(v,im,jm)
exchange2d_mpi(D,im,jm)
```

```
do i = 1, im
```

```
do j = 1, jm
```

```
elf(i,j) = elb(i,j) - 2 * dt * (
    &
    ((D(i+1,j)+D(i,j))/2 * u(i+1,j) - (D(i,j)+D(i-1,j))/2 * u(i,j)) / dx(i,j) +
    ((D(i,j+1)+D(i,j))/2 * v(i+1,j) - (D(i,j)+D(i,j-1))/2 * v(i,j)) / dy(i,j))
```

787

788 Figure 1. Implementation of Eq. (4) by basic operators. The *elf* and *elb* are the surface

789 elevations at times $(t+1)$ and $(t-1)$ respectively.

790



\$ Equation (8)

$$elf = elb - 2 * dt * (DXF(AXB(D) * U) + DYF(AYB(D) * V))$$

\$ Equation (9)

$$Uf = Db * Ub / Df - 2 * dt / Df * (DXB(AXF(AXB(D) * U) * AXF(U)) + DYF(AXB(AYB(D) * V) * AYB(U)) - & \\ AXB(f * AYF(V) * D) + g * AXB(D) * DXB(el) - aam * AXB(D) * (DXB(DXF(Ub)) + DYF(DYB(Ub)))))$$

\$ Equation (10)

$$Vf = Db * Vb / Df - 2 * dt / Df * (DXF(AYB(AXB(D) * U) * AXB(V)) + DYB(AYF(AYB(D) * V) * AYF(V)) + & \\ AYB(f * AXF(U) * D) + g * AYB(D) * DYB(el) - aam * AYB(D) * (DXF(DXB(Vb)) + DYB(DYF(Vb)))))$$

791

792 Figure 2. Implementation of the shallow water equations by basic operators. *elf*, *el* and

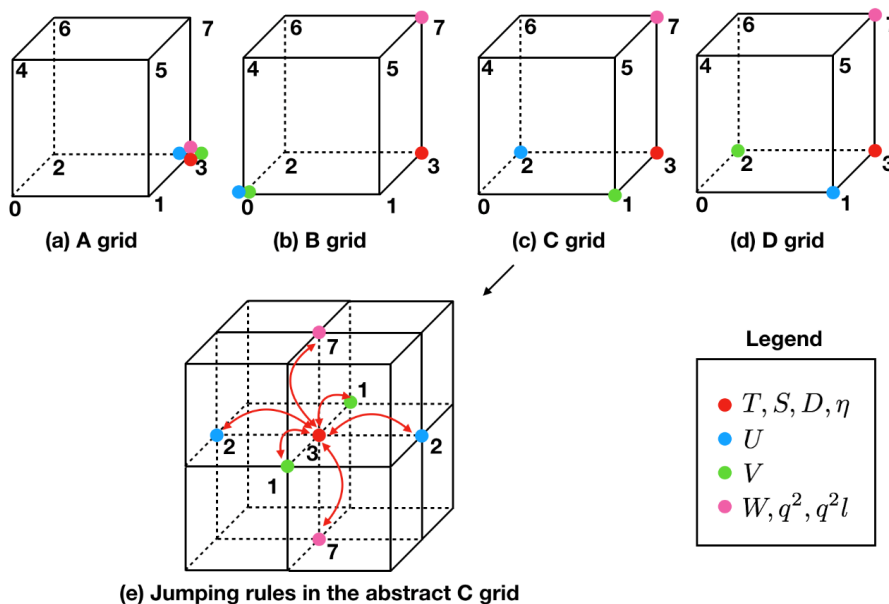
793 *elb* denote sea surface elevations at times $(t+I)$, t and $(t-I)$, respectively. *Uf*, *U* and *Ub*

794 denote the zonal velocity at times $(t+I)$, t and $(t-I)$, respectively. *Vf*, *V* and *Vb* denote

795 the meridional velocity at times $(t+I)$, t and $(t-I)$, respectively. *aam* denotes the

796 viscosity coefficient.

797



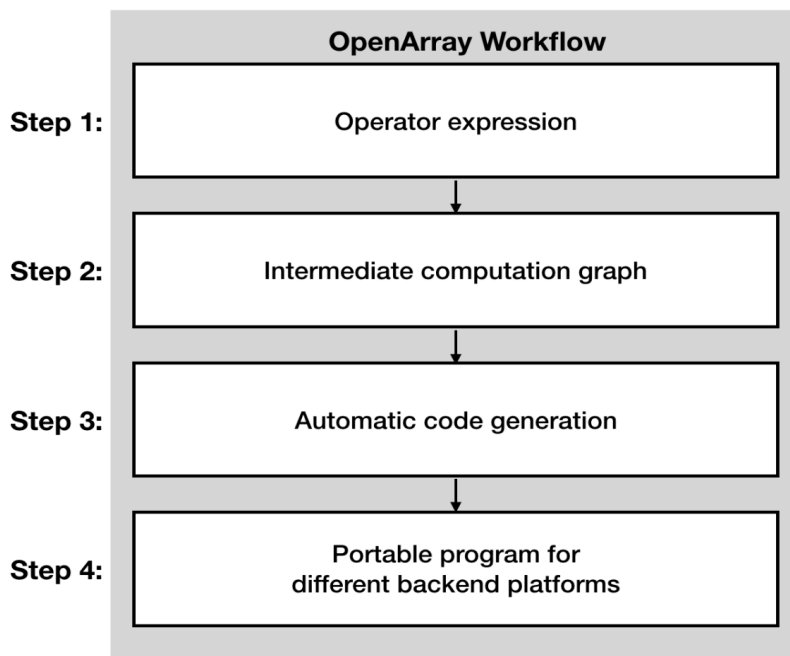
798

799

Figure 3. The schematic diagram of the relative positions of the variables on the abstract staggered grid and the jumping procedures among the grid points.

800

801



802

803

804

Figure 4. The workflow of OpenArray.



Formula	$\eta_{t+1} = \eta_{t-1} - 2 * dt * \left(\delta_f^x(\bar{D}_b^x * U) + \delta_f^y(\bar{D}_b^y * V) \right)$
Code	$elf = elb - dt2 * (DXF(AXB(D)*U) + DYF(AYB(D)*V))$

805

806

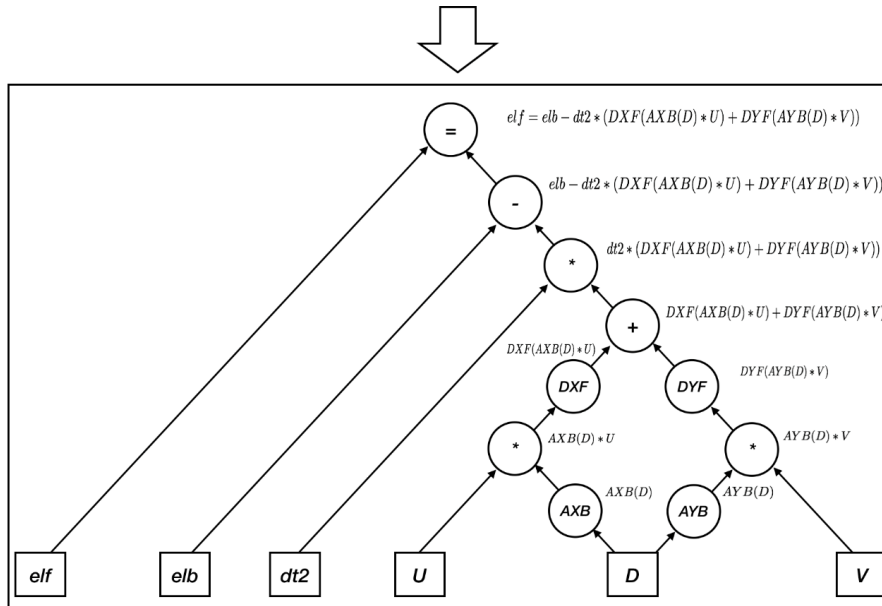
807

808

Figure 5. The effect of “The self-documenting code is the formula” illustrated by the sea surface elevation equation.



$$elf = elb - dt2 * (DXF(AXB(D) * U) + DYF(AYB(D) * V))$$



809
 810
 811

Figure 6. Parsing the operator expression form into the computation graph.

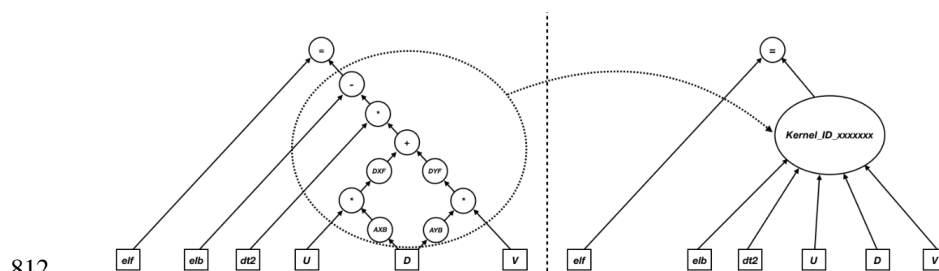
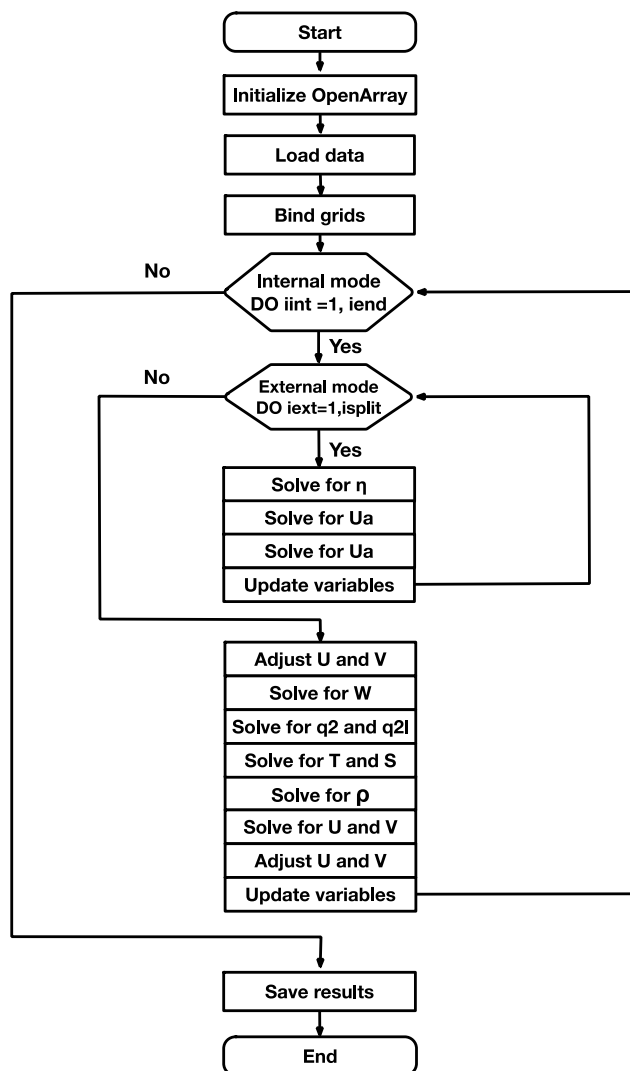
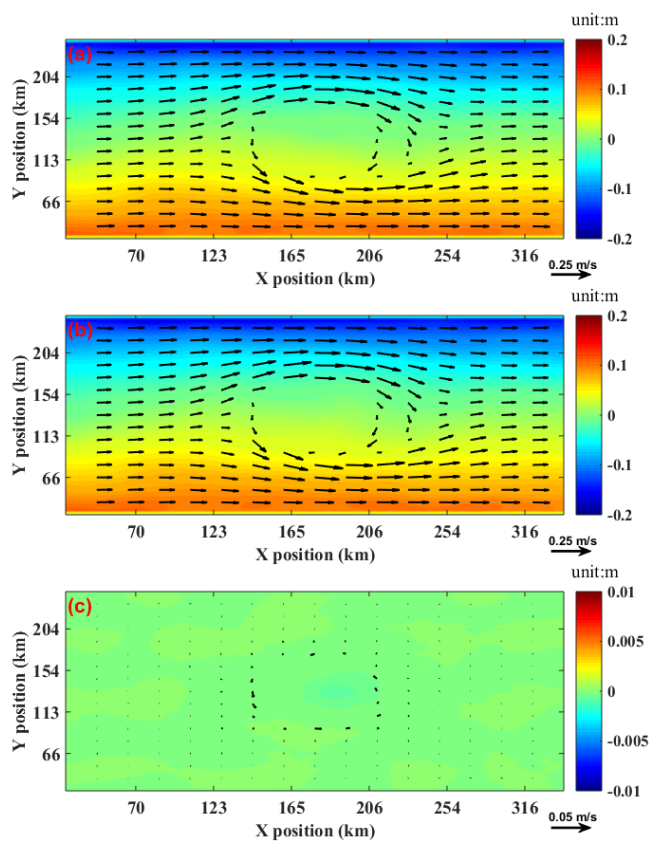


Figure 7. The schematic diagram of kernel fusion.

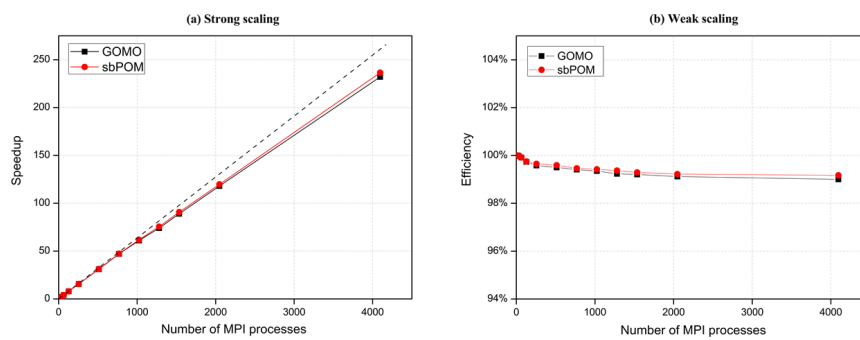


815
816
817

Figure 8. Flow diagram of GOMO



818
819 Figure 9. Comparison of the surface elevation (shaded) and currents at 3500 metres
820 depth (vector) between GOMO and sbPOM on the 4th model day. (a) GOMO, (b)
821 sbPOM, (c) GOMO-sbPOM.
822



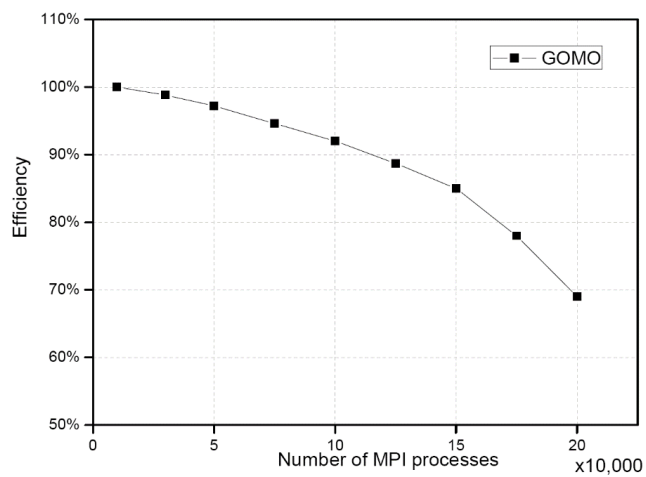
823

824 Figure 10. Performance comparison between sbPOM and GOMO. (a) The strong

825 scaling result; vertical axis denotes the speedup relative to 16 processes in a single node.

826 (b) The weak scaling result.

827



828

829

Figure 11. Parallel efficiency of GOMO on the Sunway TaihuLight supercomputer.

830